Journal of Fluorine Chemistry 141 (2012) 69–75

Contents lists available at SciVerse ScienceDirect

Journal of Fluorine Chemistry

journal homepage: www.elsevier.com/locate/fluor

Multifunctional surface modification of an aramid fabric via direct fluorination

Euigyung Jeong [a], Bum Hoon Lee [b], Song Jun Doh [c], In Jun Park [d], Young-Seak Lee [a,*]

[a] Department of Fine Chemical Engineering and Applied Chemistry, BK21-E²M, Chungnam National University, Daejeon 305-764, Republic of Korea
[b] Heracron Research Institute, Kolon Industries, Inc., 212 Gongdan-dong, Gumi-Si, Gyungsangbuk-do 730-030, Republic of Korea
[c] Department of Textile Convergence of Biotechnology & Nanotechnology, Convergence Technology R&D Division, Korea Institute of Industrial Technology, 1271-18 Sa-3-dong, Sangrok-gu, Ansan-si Gyounggi-do 426-791, Republic of Korea
[d] Research Center for Biorefinery, Korea Research Institute of Chemical Technology, Daejeon 305-600, Republic of Korea

ARTICLE INFO

Article history:
Received 26 February 2012
Received in revised form 6 June 2012
Accepted 12 June 2012
Available online 19 June 2012

Keywords:
Aramid
Direct fluorination
Hydrophobicity
Oleophobicity
Resin impregnation

ABSTRACT

This study investigated the potential of direct fluorination as a multifunctional surface modification method for an aramid fabric. The aramid fabric was fluorinated at temperatures of 30, 90, and 150 °C. As the fluorination temperature increased, the fluorinated aramid fabric became more hydrophobic and oleophobic, with a water contact angle of 129.3° and a diiodomethane contact angle of 108.6° when the fluorination temperature was 150 °C. Thus, the fluorinated fabric could be defined as an omniphobic surface. Both the phenol resin wettability and the impregnation of the fluorinated aramid fabric improved as the fluorination temperature increased, suggesting better interfacial adhesion between the fabric and the polymer matrix. Direct fluorination of an aramid fabric can be an efficient multifunctional surface modification method to achieve omniphobicity in the aramid fabric for the protection, self-cleaning, and improved interfacial adhesion between the fabric and resin for fiber-reinforced polymer composites.

1. Introduction

Aramid fibers have attracted the attention of many researchers because of their stiffness, high strength, high fracture strain, excellent thermal stability, chemical inertness, and low density [1,2]. Therefore, aramid fabrics are promising candidates for applications as protective wear (such as bulletproof vests) and as a reinforcement fiber for advanced composites [3–5].

When an aramid fabric is used for protective wear, its wetting behavior is one of the most important factors, because the water in the protective fabric impairs its protective performance because of the reduction in the friction between the yarns [6,7]. In addition, highly hydrophobic and/or oleophobic surfaces (also denoted as omniphobic surfaces when the surface is both hydrophobic and oleophobic) are desirable for many applications, including self-cleaning surfaces [8–10].

When an aramid fabric is used as reinforcement for advanced composites, the aramid fiber has poor interfacial adhesion with almost all of the commercially available resins because it has a smooth surface and is chemically inert [11]. Because the mechanical properties of fiber-reinforced polymer composites depend on both the mechanical properties of the reinforcement and matrix and the interfacial adhesion between them, it is necessary to improve the interfacial adhesion of the aramid fabric [12].

Several methods can be used to improve the hydrophilicity, oleophobicity, and interfacial adhesion of the aramid fabric. Chemical treatment [13–15], plasma treatment [16–18], and even ultrasonic treatment [19] can be used. Direct fluorination can be an effective method to simultaneously improve the omniphobicity and interfacial adhesion with little damage to the polymer [20,21]. Moreover, fluorination is dry and uses no water or organic solvents, which are cost-, energy-, and time-consuming and may lead to water pollution [22].

This study investigated the potential of direct fluorination as a multifunctional surface modification method for improved hydrophobicity and oleophobicity, resulting in improved omniphobicity and improved interfacial adhesion between the fiber and the matrix polymer. The effect of fluorination on the omniphobicity of the aramid fabric was assessed, and the phenol resin wettability and impregnation of the fluorinated aramid fabric were also investigated to evaluate the potential interfacial adhesion between the fabric and the polymer matrix.

2. Results and discussion

2.1. The surface chemical composition of the untreated and fluorinated aramid fabrics

The surface chemical composition of the untreated and fluorinated aramid fabrics was characterized using XPS analysis. The resulting elemental analysis results are shown in Table 1. The

* Corresponding author. Tel.: +82 42 821 7007; fax: +82 42 822 6637.
E-mail addresses: youngslee@cnu.ac.kr, wolfpack@cnu.ac.kr (Y.-S. Lee).

0022-1139/$ – see front matter © 2012 Elsevier B.V. All rights reserved.
http://dx.doi.org/10.1016/j.jfluchem.2012.06.010

Table 1
The XPS surface elemental analysis parameters of the aramid fabrics.

Samples	Elemental contents (atomic %)				N/C	O/C	F/C
	C1s	N1s	O1s	F1s			
Untreated	82.0	5.0	13.0	0.00	0.06	0.16	0.00
F30	61.5	6.8	12.0	19.7	0.11	0.20	0.32
F90	49.4	6.2	12.1	32.3	0.13	0.24	0.65
F150	45.3	5.4	10.1	39.2	0.12	0.22	0.87

major surface constituents of the untreated aramid fabric were carbon, oxygen, and nitrogen, as predicted by the chemical structure of the aramid polymers. And the new major surface constituent, fluorine, was observed in the fluorinated aramid fabrics. When comparing the fluorine content and F/C ratio of each sample, the surface fluorine concentration increased, as the fluorination temperature increased. The chemical bonds of the untreated and fluorinated aramid fabrics were investigated via C1s deconvolution. The results are depicted in Fig. 1, and the concentrations of the functional groups of the aramid fabrics are shown in Table 2. The constituents that were observed in the untreated aramid fabric were 1, 2, 3, and 4 at 285.0, 286.3, 287.8, and 289.1 eV, respectively, as shown in Fig. 1(a). These corresponded to C–C, C–N/C–O, O=C–N–H, and O=C–O, respectively, as previously reported [23,24]. After fluorination, a new constituent, 5, was observed in F30, F90, and F150 at 290.3 eV, as shown in Fig. 1(b)–(d). This constituent corresponded to covalent C–F, which is from CF, CF_2 or the least possibly CF_3, as previously reported [29–32]. As in the elemental analysis of the survey spectra, the C–F bond concentration increased as the fluorination temperature increased from 30 (F30) to 90 (F90) to 150 °C (F150). F30 had an O=C–O concentration that was similar to the concentration in the untreated fabric, whereas F90 and F150 had significantly increased O=C–O concentrations. When fluorination was performed at the relatively higher fluorination temperatures of 90 or 150 °C, the amide bonds of the aramid polymer might have been partially broken and formed carboxylic acid groups (O=C–O). Fluorination at a higher fluorination temperature seems to introduce more fluorine, but the fluorination reaction apparently breaks some of the amide bonds.

The F1s deconvolution spectra of the fluorinated aramid fabrics are shown in Fig. 2 and confirmed the nature of the C–F bonds. Only covalent C–F bonds were observed in all of the spectra of the fluorinated aramid fabrics. The fluorinated surfaces of the aramid fabrics are expected to be hydrophobic and oleophobic.

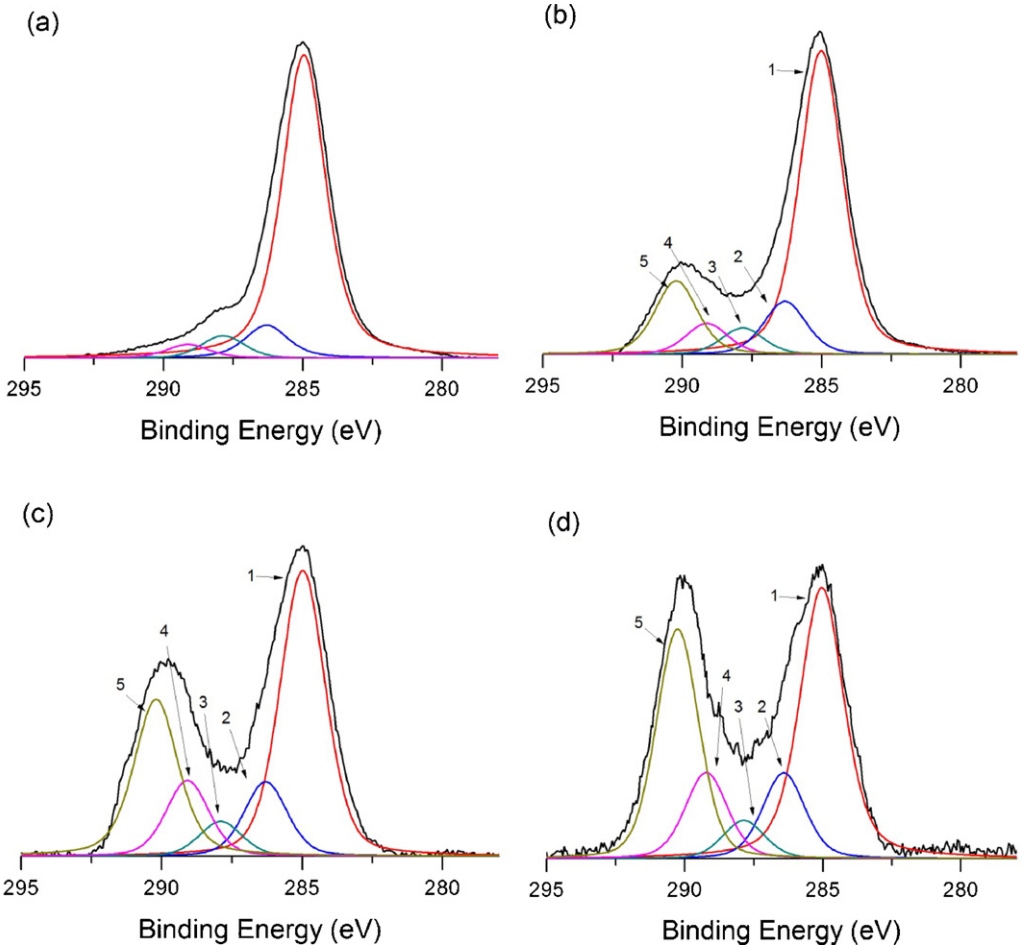

Fig. 1. The C1s spectra of the untreated and fluorinated aramid fabrics: (a) untreated, (b) F30, (c) F90, and (d) F150.

Table 2
The concentrations of the functional groups of the aramid fabrics.

Samples	Concentration (%)				
	C–C	C–N/C–O	O=C–N–H	O=C–O	C–F
	285.0 eV	286.3 eV	287.8 eV	289.1 eV	290.2 eV
Untreated	82.5	8.8	5.2	3.5	–
F30	63.3	10.5	5.2	6.1	14.9
F90	45.9	11.3	5.3	11.5	25.9
F150	41.0	11.7	5.2	11.7	30.4

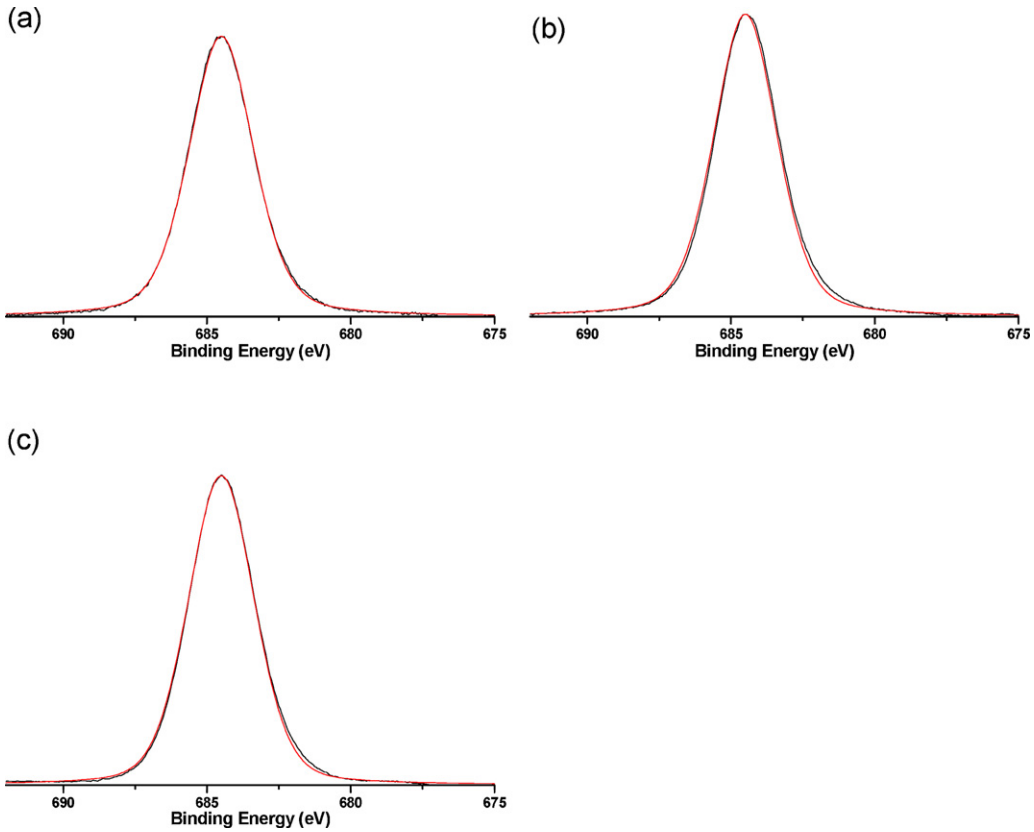

Fig. 2. The F1s spectra of the fluorinated aramid fabrics: (a) F30, (b) F90, and (c) F150.

2.2. The bulk chemical composition of the untreated and fluorinated aramid fabrics

Because XPS only provides the surface chemical compositions of the materials, FTIR analysis (4000–650 cm^{-1}) was performed to characterize the bulk chemical composition of the untreated and fluorinated aramid fabrics. Fig. 3 depicts the FTIR spectra of the aramid fabric samples. The characteristic bands of the aramid polymer (N–H stretching, C=O stretching, C–N stretching, N–H bending of the amide moiety, and C–H deformation and bending of the aromatic ring) were observed in all of the samples [12]. After the fluorination of the aramid fabrics, the C–F stretching bands of the C–F bonds were observed in the range of 1000–1300 cm^{-1} [5,12]. When comparing the spectra of the fluorinated samples, the C–F peak intensity increased as the fluorination temperature increased. In addition, the C=O stretching bands of the carboxylic acid groups appeared when the fluorination temperature was higher (90 and 150 °C). Some amide bond cleavage might have occurred and resulted in the increased formation of carboxylic acid groups and C–F bonds during fluorination at higher temperatures. The difference in the intensities of the C–F peaks was relatively small when the untreated and fluorinated aramid fabrics were compared and especially when the untreated aramid fabric and F30 were compared. Due to the chemical stability and highly crystalline nature of the aramid polymer, it is hard to be fluorinated and the resulting fluorinated aramid is very thin. Because the intensities of the FTIR spectra are proportional to the thickness according to Beer's law, the resulting C–F peak intensity of F30 is very weak. However, when the fluorination temperature was higher (at 90 °C or 150 °C), the thickness of the fluorinated layer also increased. Therefore, the C–F peak intensities of F90 and F150 were much stronger than the peak intensity of F30. In other words, F90 and F150 had thicker fluorinated layers, resulting in the stronger C–F peaks. The carboxylic acid peak was much weaker than the other characteristic peaks of the aramid, suggesting that only a small number of the surface amide groups of the aramid polymer were broken. The bulk properties of the aramid were retained even with the higher surface fluorine level, as shown in the results of the XPS analysis after fluorination at a higher temperature.

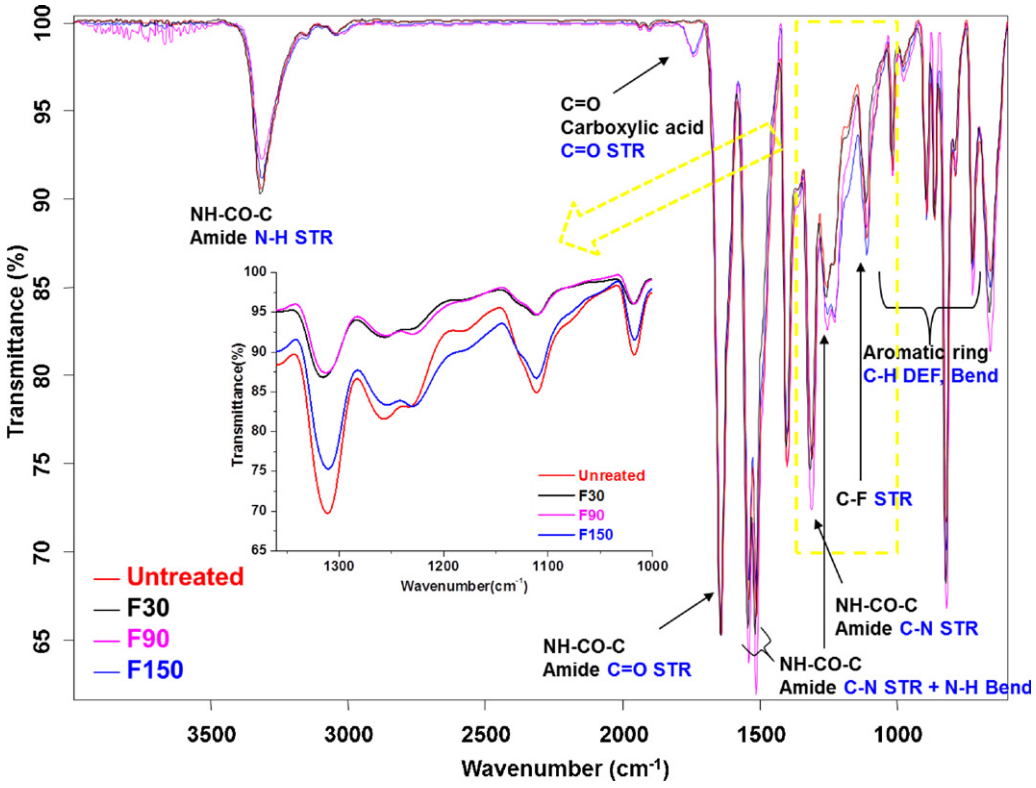

Fig. 3. The FTIR spectra of the aramid fabrics and their expansions between 1000 and 1300 cm^{-1}.

2.3. The morphologies of the untreated and fluorinated fabrics

The morphologies of the aramid fabrics were investigated using SEM analysis. Fig. 4 depicts SEM images of the samples. Fig. 4(a) shows that the aramid fabric was a plain-woven fabric with a 656–698 μm yarn diameter that consisted of fibers with a 12.3–13.5 μm diameter. Fig. 4(b)–(d) shows the surface morphology of the untreated and fluorinated aramid fibers. F30 had a surface morphology similar to that of the untreated aramid fabric, which had a smooth and clean surface. F90 had a slightly irregular

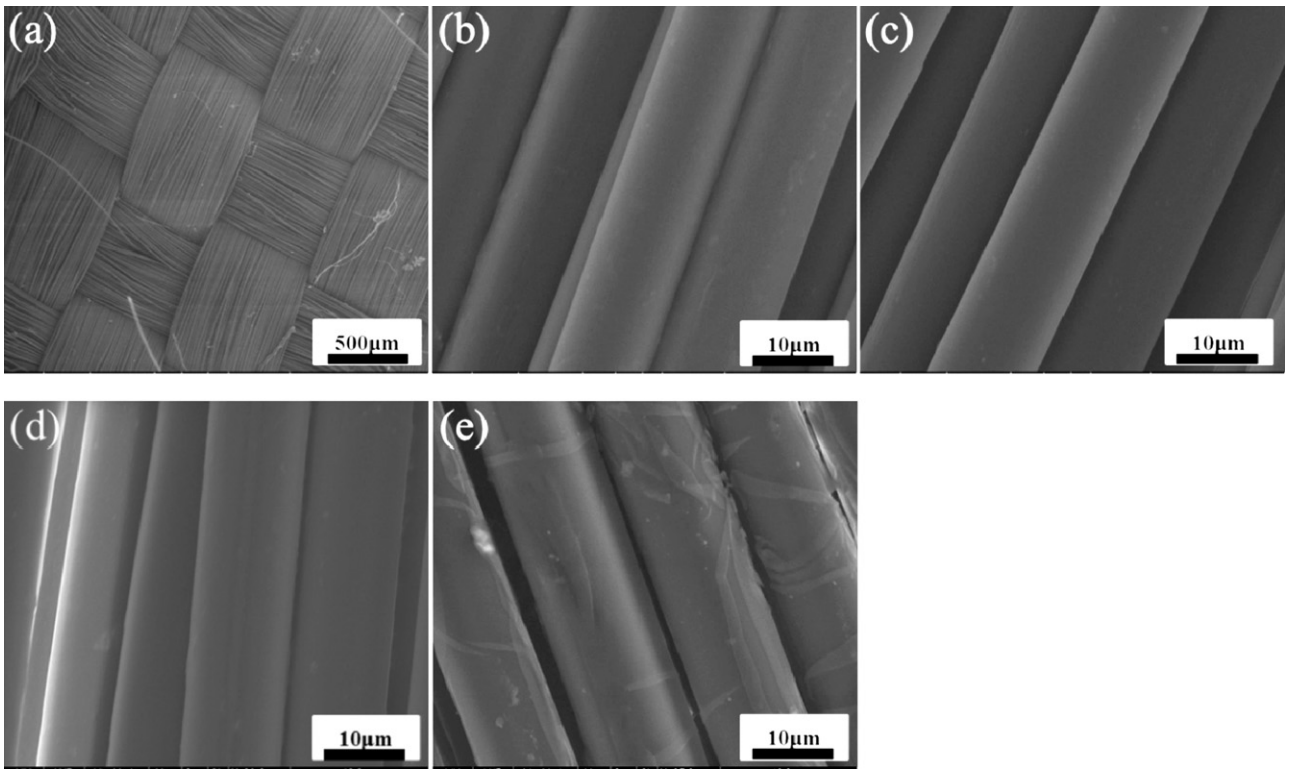

Fig. 4. SEM images of the aramid fabrics: (a) the fabric structure and fiber surfaces of the (b) untreated, (c) F30, (d) F90, and (e) F150 fabrics.

Table 3
The contact angles of the liquids on the aramid fabrics.

	Water contact angle (°)	Diiodomethane contact angle (°)
Untreated	0	0
F30	0	0
F90	116.8(±2.5)	99.3(±2.9)
F150	129.3(±2.1)	108.6(±1.0)

surface, and F150 had a roughened fiber surface. Based on the XPS and FTIR data, F150 had the highest surface fluorine content and the thickest fluorinated layer of the fluorinated samples, yet the fluorinated layer was thinner than the unfluorinated layer. The roughness arising from high-temperature fluorination through hyperfluorination of the aromatic groups or the breakage of the amid groups was expected to improve the hydrophobicity, oleophobicity (omniphobicity), and resin wettability of the aramid fabric surface without losing its beneficial bulk physical properties.

2.4. The omniphobicity of the untreated and fluorinated fabrics

The surface wettability of the aramid fabrics was investigated by contact angle measurements using water and diiodomethane. Table 3 depicts the contact angles of the liquids on the aramid fabric samples. The untreated aramid fabric absorbed both water and diiodomethane immediately upon contact. F30 also absorbed both water and diidomethane, but the absorption time of the liquids was about 3–5 s. Even though the liquid absorption times were different, both the untreated aramid fabric and F30 are hydrophilic and oleophilic. F90 was hydrophobic and oleophobic, with a water contact angle of 116.8° (±2.5°) and a diiodomethane contact angle of 99.3° (±2.9°). F150 was even more hydrophobic and oleophobic, with a water contact angle of 129.3° (±2.1°) and a diiodomethane contact angle of 108.6° (±1.0°). Both F90 and F150 could be considered omniphobic based on the results of the contact angle measurements.

Table 4
The surface free energies of the liquids used.

	γ_{total} (mN/m)	γ_l^p (mN/m)	γ_l^d (mN/m)
Water	72.3	51.0	21.3
Diiodomethane	50.8	1.3	49.5

Table 5
The calculated surface free energies of the aramid fabrics.

	γ_{total} (mN/m)	γ_s^d (mN/m)	γ_s^p (mN/m)
F90	8.3	7.5	0.8
F150	5.8	5.7	0.1

The surface free energies of the aramid samples can be calculated from the contact angles measured with water and diiodomethane. The following Eqs. (1) and (2) from the Owens–Wendt geometric mean method were used [34]:

$$\gamma_l(1+\cos\theta) = 2\sqrt{\gamma_s^p\gamma_l^p} + 2\sqrt{\gamma_s^d\gamma_l^d} \quad (1)$$

$$\gamma_{sl} = \gamma_s + \gamma_l - 2\sqrt{\gamma_s^p\gamma_l^p} - 2\sqrt{\gamma_s^d\gamma_l^d} \quad (2)$$

where θ is the contact angle between the aramid fabric and the testing liquid on which the measurement was performed, γ_l is the surface tension of the testing liquid, γ_s^p and γ_l^p are the polar

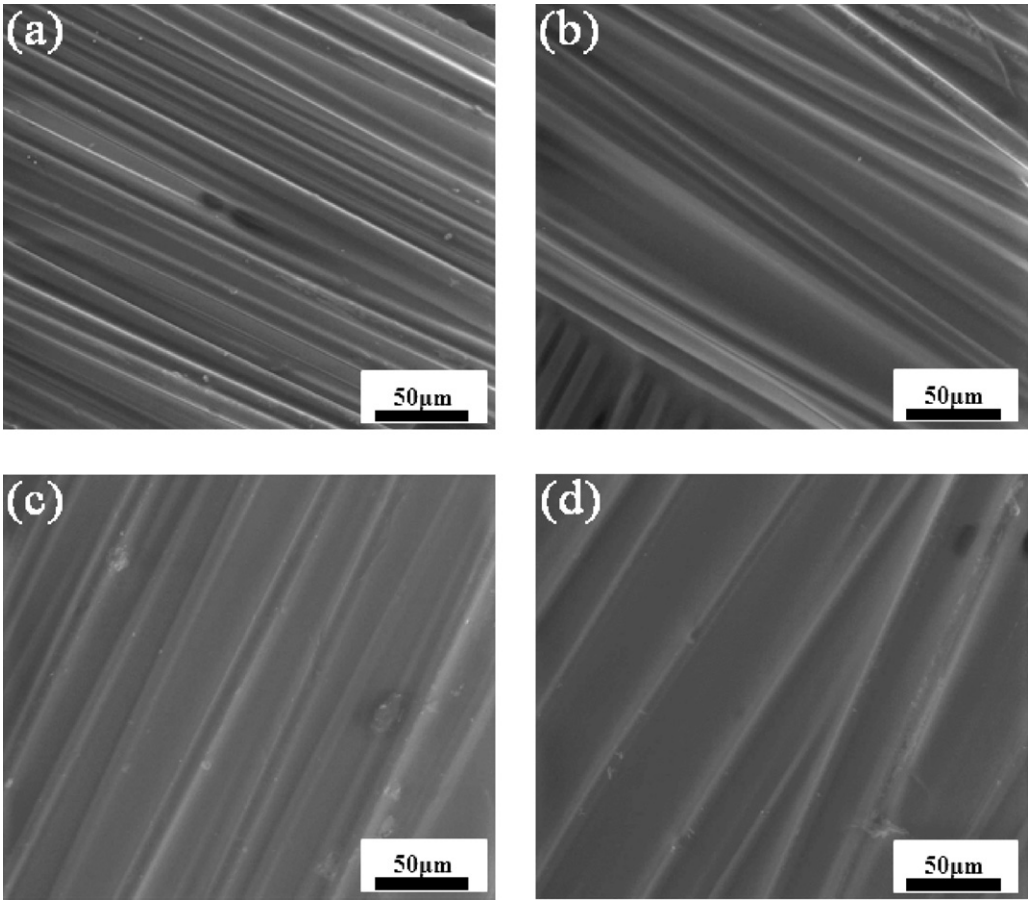

Fig. 5. Phenol resin wettability of the aramid fabrics: (a) untreated, (b) F30, (c) F90, and (d) F150.

components of the total surface free energy of the fabric and liquid, respectively, γ_s^d and γ_l^d are the dispersive components of the total surface free energy of the fabric and liquid, respectively.

The surface free energies of water and diiodomethane are shown in Table 4, and the calculated surface free energies of the aramid fabrics are shown in Table 5. Because the untreated sample and F30 absorbed both water and diidomethane, the surface free energies could not be calculated. The untreated sample and F30 have distinctly high surface free energies. F90 had a significantly decreased total surface free energy of 9.1 mN/m. F150 had an even more significantly decreased total surface free energy of 5.9 mN/m. Based on the XPS and FTIR results, F90 had twice the fluorine content of F30. This difference in the surface fluorine content seems to be responsible for the significantly improved omniphobicity of F90. In addition, F150 had three times the fluorine content of F30 and a roughened fiber surface that was induced by the higher-temperature fluorination. Due to the synergistic effect of the elevated fluorine content and the roughened fiber surface, F150 had an even more significantly decreased surface free energy, which resulted in the most omniphobic sample surface.

2.5. The phenol resin wettability and impregnation of the untreated and fluorinated aramid fabrics

The phenol resin wettability of the untreated and fluorinated aramid fabrics was evaluated using the SEM images that were obtained from the fabrics that had been dipped into the mixture of phenol resin and methanol (50/50, w/w). The SEM images of the samples are shown in Fig. 5. As shown in Fig. 5, the surface of the phenol resin-dipped fabric became smoother because the grooves formed by the fibers were filled with the phenol resin. When the aramid fabric was fluorinated at higher temperatures, the surface of the dipped fabric became smoother with more filled grooves. More phenol resin was apparently attached to the surface of the aramid fabric when the fabric was fluorinated at a higher temperature. This was attributed to the fluorine-related functional groups that were reported to form electrophilic bonds with oxygen- and nitrogen-related functional groups such as –OH and –NH_2 [25–27]. These bonds improved the interfacial affinity of the fluorinated aramid fabrics to the –OH-rich phenol resin, resulting in a wetter resin and smoother surface for the dipped fabrics. The improved roughness of the F150 surface induced by fluorination also contributed to the wetting of the resin, resulting in the smoothest surface out of all of the evaluated samples.

The phenol resin impregnation of the untreated and fluorinated aramid fabrics was also evaluated using SEM images obtained from a cross-section of the phenol resin-impregnated fabrics, which were cut by focused ion beam (FIB). The SEM images of the resin-impregnated fabrics are shown in Fig. 6. The voids between the aramid fibers were filled with the phenol resin after impregnation. The number of these voids decreased as the fluorination temperature of the fabric increased. The surface chemical composition of the fluorinated fabric showed that more fluorine-related surface groups were introduced onto the surface of the fabric as the fluorination temperature increased. With more fluorine-related functional groups present, the resin impregnation into the aramid fabric improved because of the reduced abrasion of the interface between the aramid fiber and the phenol resin. The presence of surface fluorine-related functional groups usually reduces abrasion [25].

3. Conclusions

An aramid fabric was fluorinated at temperatures of 30 °C, 90 °C, and 150 °C to investigate the effectiveness of the direct

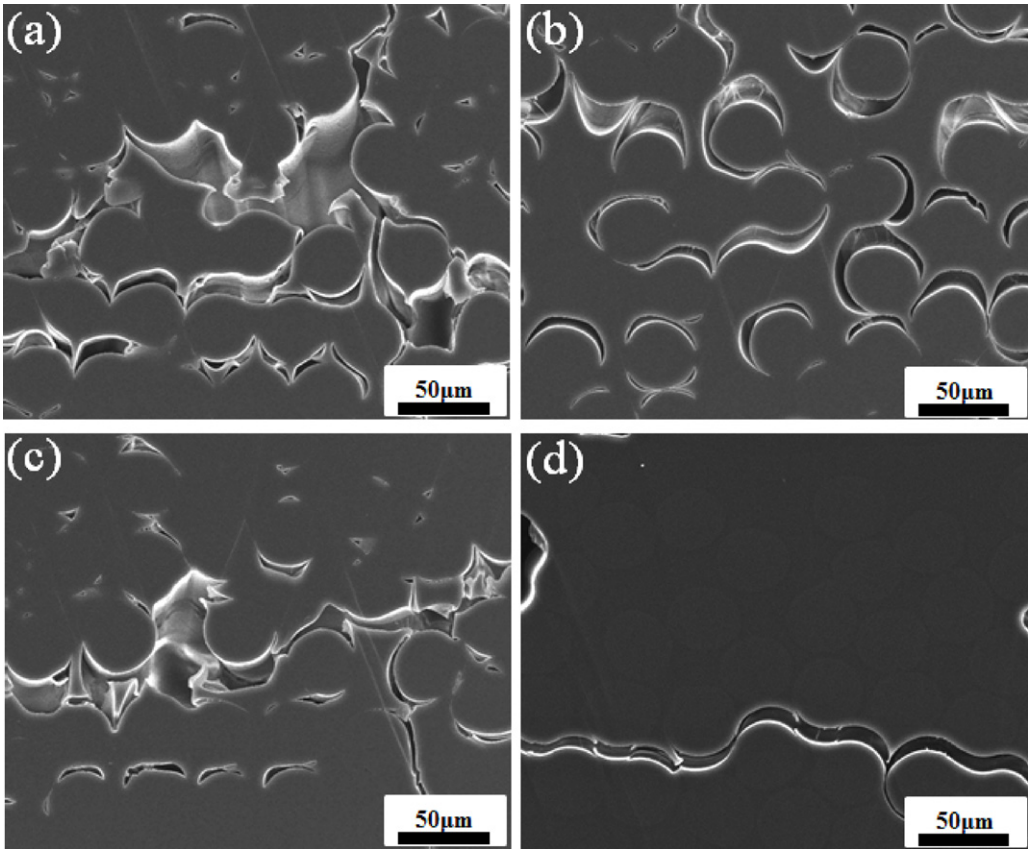

Fig. 6. Phenol resin impregnation of the aramid fabrics: (a) untreated, (b) F30, (c) F90, and (d) F150.

fluorination as a multifunctional surface modification method. As the fluorination temperature increased, the fluorinated aramid layers became thicker, and more surface fluorine-related functional groups were observed. The surface morphology of the aramid fiber became rougher when the fluorination temperature was 150 °C. The fluorinated aramid fabric became more hydrophobic and oleophobic, with a water contact angle of 129.3° and a diiodomethane contact angle of 108.6° when the fluorination temperature was 150 °C. The surface of the fluorinated aramid fabric could be defined as an omniphobic surface. Both the phenol resin wettability and the impregnation of the fluorinated aramid fabric improved as the fluorination temperature increased, suggesting better interfacial adhesion between the fabric and the polymer matrix. Therefore, direct fluorination of the aramid fabric can be an efficient multifunctional surface modification method to achieve omniphobicity in the aramid fabric for protection, self-cleaning, and improved interfacial adhesion between the fabric and the resin for fiber-reinforced polymer composites.

4. Experimental

4.1. Materials

The aramid fibers used in this study were Kevlar® K1200, which are manufactured by DuPont. The phenolic resin (KRD-HM2) was supplied by Kolon Chemicals, Korea. Fluorine (Messer Griesheim GmbH, 99.8%) and nitrogen (99.999%) gases were used for the direct fluorination of the aramid fabric.

4.2. Fluorination of the aramid fabric

Fluorination was performed using a fluorination apparatus that consisted of a reactor, a vacuum pump, and gas cylinders connected to a buffer tank. A detailed description of the fluorination apparatus has been provided previously [28–29,33,34]. The aramid fabric was loaded into a nickel boat inside the reactor and degassed to remove any impurities. The fluorination of the aramid fabric was then performed at 30, 90, and 150 °C for 30 min at a fluorine pressure of 0.1 bar and a nitrogen pressure of 0.9 bar. The aramid fabric was degassed to remove any unreacted gas after the fluorination. The samples were designated F30, F90, and F150, depending on the fluorination temperature.

4.3. Characterization of the fluorinated aramid fabric

X-ray photoelectron spectroscopy (XPS) spectra of the aramid fabrics were obtained with a MutiLab 2000 spectrophotometer (Thermo Electron Co., England) to investigate the changes in the chemical composition of the surfaces before and after fluorination using Al Kα (1485.6 eV) X-rays with a 14.9-keV anode voltage, a 4.6-A filament current, and a 220-mA emission current. All of the samples were pretreated at 10^{-9} mbar to remove any impurities. The XPS survey spectra were obtained with a 50-eV pass energy and a 0.5-eV step size. The core level spectra were obtained at a 20-eV pass energy with a step size of 0.05 eV. FWHM of each component was 1.8 eV. Fourier transform infrared spectroscopy (FTIR; Bruker Optics IFS 66/S; reflectance ATR mode; 64 scans) was used to characterize the bulk chemical composition of the aramid fabrics before and after fluorination.

Scanning electron microscopy (SEM; JEOL, JSM-7000F, Japan) was used to investigate the changes in the morphologies of the aramid fabrics. The phenolic resin wettability and the impregnation of the aramid fabric were also evaluated using SEM images. Next, the untreated and fluorinated aramid fabrics were dipped into the mixture of phenol resin and methanol (50/50, w/w), dried and completely cured at 80 °C for 4 h to evaluate the phenol resin wettability. Next, the untreated and fluorinated aramid fabrics were impregnated with phenol resin for 10 s, dried, and completely cured at 80 °C for 4 h to evaluate the phenol resin impregnation.

The contact angles of the aramid fabrics were measured using drop-shape analysis (DSA; DSA 100, Krűss), and the surface energies were calculated from the measured contact angles using the Owens–Wendt geometric mean method [35].

Acknowledgements

This research was supported by a grant from the Fundamental R&D Program for Core Technology of Materials and funded by the Ministry of Knowledge Economy, Republic of Korea.

References

[1] S. Zhang, G. He, G. Liang, H. Cui, W. Zhang, B. Wang, Applied Surface Science 256 (2010) 2104–2109.
[2] A.A. Leal, J.M. Deitzel, S.H. McKnight, J.W. Gillespie Jr., Polymer 50 (2009) 1228–1235.
[3] Y. Wang, Y. Miao, D. Swenson, B.A. Cheeseman, C. Yen, B. LaMattina, International Journal of Impact Engineering 37 (2010) 552–560.
[4] G. Li, C. Zhang, Y. Wang, P. Li, Y. Yu, X.H. Liu, X. Yang, Z. Xue, S. Ryu, Composites Science and Technology 68 (2008) 3208–3214.
[5] J. Maity, C. Jacob, C.K. Das, S. Alam, R.P. Singh, Composites Part A: Applied Science and Manufacturing 39 (2008) 825–833.
[6] S. Bazhenov, Journal of Materials Science 32 (1997) 4167–4173.
[7] F.A. Reifler, E.H. Lehmann, G. Frei, H. May, R. Rossi, Measurement Science and Technology 17 (2006) 1925–1934.
[8] K. Autumn, Y.A. Liang, S.T. Hsieh, W. Zesch, W.P. Chan, T.W. Kenny, R. Fearing, R.J. Full, Nature 405 (2000) 681–685.
[9] X. Feng, L. Jiang, Advanced Materials 18 (2006) 3063–3078.
[10] T. Darmanin, F. Guittard, Journal of Colloid and Interface Science 335 (2009) 146–149.
[11] C. Jiang, P. Chen, W. Liu, B. Li, Q. Wang, Applied Surface Science 257 (2011) 4165–4170.
[12] J. Maity, C. Jacob, C.K. Das, A.P. Kharitonov, R.P. Singh, S. Alam, Polymer Composites 28 (2007) 462–469.
[13] P.A. Tarantili, A.G. Andreopoulos, Journal of Applied Polymer Science 65 (1997) 267–276.
[14] M. Breznick, J. Banhaji, H. Guttmann, G. Marom, Polymer Communications 28 (1987) 55–56.
[15] A.G. Andrepoulos, Journal of Applied Polymer Science 38 (1989) 1053–1064.
[16] Y. Ren, C. Wang, Y. Qiu, Applied Surface Science 253 (2007) 9283–9289.
[17] Y.J. Hwang, Y. Qiu, C. Zhang, B. Jarrard, R. Stedeford, J. Tsai, Y.C. Park, M. McCord, Journal of Adhesion Science and Technology 17 (2003) 847–860.
[18] P. Chen, J. Wang, B. Wang, W. Li, C. Zhang, H. Li, B. Sun, Surface and Interface Analysis 41 (2009) 38–43.
[19] L. Liu, Y.D. Huang, Z.Q. Zhang, Z.X. Jiang, L.N. Wu, Applied Surface Science 254 (2008) 2594–2599.
[20] A.P. Kharitonov, Progress in Organic Coatings 61 (2008) 192–204.
[21] A.P. Kharitonov, R. Taege, G. Ferrier, V.V. Teplyakov, D.A. Syrtsova, G.-H. Koops, Journal of Fluorine Chemistry 126 (2005) 251–263.
[22] M. Xi, Y.-L. Li, S.-Y. Shang, D.-H. Li, Y.-X. Yin, Surface and Coatings Technology 202 (2008) 6029–6033.
[23] M.-J. Jung, E. Jeong, S.-I. Lee, Y.-S. Lee, Journal of Industrial and Engineering Chemistry 18 (2012) 642–647.
[24] N. Inagaki, S. Tasaka, H. Kawai, Y. Yamada, Journal of Applied Polymer Science 64 (1997) 831–840.
[25] E. Jeong, J. Kim, S.H. Cho, Y.-S. Bae, Y.-S. Lee, Journal of Fluorine Chemistry 132 (2011) 291–297.
[26] J.S. Im, J.G. Kim, S.-H. Lee, Y.-S. Lee, Colloids and Surfaces A 364 (2010) 151–157.
[27] P. Saini, V. Choudhary, B.P. Singh, R.B. Mathur, S.K. Dhawan, Materials Chemistry and Physics 113 (2009) 919–926.
[28] H.-R. Yu, J.G. Kim, J.S. Im, T.-S. Bae, Y.-S. Lee, Journal of Industrial and Engineering Chemistry 18 (2012) 674–679.
[29] M.J. Jung, E. Jeong, S. Kim, S.I. Lee, J.-S. Yoo, Y.-S. Lee, Journal of Fluorine Chemistry 132 (2011) 1127–1133.
[30] A. Tressaud, E. Durand, C. Labrugére, Journal of Fluorine Chemistry 125 (2004) 1639–1648.
[31] I. Craussous, H. Groult, F. Lantelme, D. Devilliers, A. Tressaud, C. Labrugére, M. Dubois, C. Belhomme, A. Colisson, B. Morel, Journal of Fluorine Chemistry 130 (2009) 1080–1085.
[32] H. Groult, T. Nakajima, L. Perrigaud, Y. Ohzawa, H. Yashiro, S. Komaba, N. Kumagai, Journal of Fluorine Chemistry 126 (2005) 1111–1116.
[33] J.S. Im, S.C. Kang, B.C. Bai, T.-S. Bae, S.J. In, E. Jeong, S.-H. Lee, Y.-S. Lee, Carbon 49 (2011) 2235–2244.
[34] B.C. Bae, J.G. Kim, J.S. Im, S.C. Jung, Y.-S. Lee, Carbon Letters 12 (2011) 236–242.
[35] E. Jeong, T.-S. Bae, S.-M. Yun, S.-W. Woo, Y.-S. Lee, Colloids and Surfaces A 273 (2011) 36–41.